Distribution and Diffusivity of a Hydrophobic Probe Molecule in the Interior of a Membrane: Theory and Simulation

M. L. Huertas,* V. Cruz,# J. J. López Cascales,* A. U. Acuña,# and J. García de la Torre*

*Departamento de Química Física, Facultad de Química, Universidad de Murcia, 30071 Murcia, and #Instituto de Química Física Rocasolano, Consejo Superior de Investigaciones Científicas, 28006 Madrid, Spain

ABSTRACT   We propose a simple model for the distribution of position and orientation and the diffusion of a hydrophobic probe molecule embedded in a membrane. The molecule experiences both a Maier-Saupe orienting potential as well as an enclosing potential of repulsion from the membrane walls. A statistical thermodynamics treatment of the model provides predictions of the location and orientation of the molecule within the membrane. In particular, we evaluate the order parameter of the molecule in terms of the model constants. The diffusivity of the probe is studied by Brownian dynamics simulation. For rotational diffusion, we check an available analytical approximate treatment that allows for the prediction of the dynamics in terms of equilibrium quantities. We also pay attention to quantities related to the initial and mean reorientational rate of the probe. For translational diffusion, we use the simulation results to analyze some general aspects of lateral and transversal diffusion.

INTRODUCTION

The lipidic bilayer membrane is a paradigmatic system embodying both physical complexity and biological relevance. Physical aspects such as anisotropy, order, and fluidity determine the physiological role. Conceptually, these aspects are intricately interwoven, so that an overall treatment of the membrane system, enabling the description of physical properties as well as biological function, is not yet available. In recent years a powerful approach has emerged from the field of computer simulation. Molecular and Brownian dynamics simulation techniques, with nearly atomic resolution, which were successfully applied to liquid and macromolecular systems, have been applied to model bilayer membranes. Interesting examples, among others, are the works of Berendsen and co-workers (van der Ploeg and Berendsen, 1982; Egberts and Berendsen, 1994; López Cascales et al., 1996a,b), and Pastor and co-workers (Pastor and Venable, 1988, 1994; Pastor et al., 1988; de Loof et al., 1990; Venable et al., 1993). Molecular simulation at the atomic level has an important drawback: a detailed structural description implies (because of the limitation of computational resources) that the simulation is restricted to times shorter than those that characterize some physiologically relevant events.

Alternative approaches to this problem come from the physics of continuous media. Features of the bilayer membrane can be included in this description. Thus order can be represented by mean-field orienting potentials, as usually done for liquid crystals. Similarly, hydrodynamic aspects arising from the restrictions to rotational diffusion or from the finite thickness of the bilayer can be described by simple models (Kinosita et al., 1977; Szabo, 1984; Saffman and Delbrück, 1975)

Experimentally, the bilayer membrane is often studied by means of dynamic spectroscopic techniques (Bayley and Dale, 1985). Of these, an important class is that of fluorescence anisotropy decay and related techniques (Jovin et al., 1981), which usually require the introduction of a luminescent probe molecule in the membrane (Loew, 1988). Examples of such studies are the works of Ameloot et al. (1984) and Mateo et al. (1991a,b, 1993), to name a few. Molecular probes are also introduced to monitor membrane properties by following the lateral, translational diffusivity of the probe (Galla and Sackman, 1974; Eisinger and Scarlata, 1987).

Theoretical or simulation results, on the other hand, are necessary to interpret the above-mentioned experiments. On the theoretical side, an important contribution to the analysis of rotational dynamics is the powerful approximation developed by Szabo (1984) and van der Meer et al. (1984). These authors have presented a theoretical approximate result applicable to the fluorescence anisotropy decay. This result is model independent, because it only requires the knowledge of order parameters and the diffusion coefficient of the probe.

A few but noteworthy attempts have been made to simulate the motion of small molecules within the bilayer, using molecular dynamics with atomic resolution (see, for instance, Basolino-Klimas et al., 1993; and Lopez Cascales et al., 1996a,b). This approach has the advantage of being based on an essentially molecular description but, as mentioned above, it suffers badly from the limitation in the accessible time scale. Actually, we show in this paper how the description of translational and rotational dynamics requires the determination on long time tails of the correlation functions. Unfortunately, this is not possible, because of the short length of trajectories from molecular dynamics.

On the other hand, we have the alternative approach of computer simulation of models of the probe-membrane system. The models can be still simple, lacking molecular detail, and their dynamics can be described by the laws of Brownian motion. This allows us to easily reach the time scale where the diffusive processes take place in biological membranes. Thus, the Brownian dynamics (BD) simulation technique can be used for predictive purposes when theory is not available, or to test theoretical approaches (López Martínez and García de la Torre, 1987; Pastor and Szabo, 1992, 1994). In this work we apply the BD simulation to a model of the probe-membrane system that, in spite of its naive aspect, includes the most important features of the problem. Theoretical analysis and simulation work with this model provide an insight into the effect of various aspects of this system that influence the dynamics, separating out their contributions. The conclusions will be applicable to the interpretation of results from more sophisticated molecular dynamics simulation and laboratory experiments.

MODEL, THEORY, AND METHODS

Probe and membrane models

The probe-membrane system is depicted in Fig. 1. The probe is, in principle, an axisymmetric molecule (not necessarily rodlike) embedded in the membrane, which acts as an orienting environment. This interaction is characterized by means of a Maier-Saupe potential, given by

$$V_{orient}(\theta) = -kT \frac{3}{2} K_\theta(\cos^2 \theta - 1), \qquad (1)$$

where θ is the angle formed by the molecular axis and the laboratory z axis, which coincides with the normal to the membrane. kT is the thermal energy and K_θ is the constant that determines the strength of the potential. V_{orient} is the maximum for the perpendicular orientation, $\theta = \pi/2$, and the minimum for $\theta = 0$ and $\theta = \pi$.

The membrane is finite in the z direction, with height h. No part of the molecule can trespass the boundaries of the membrane, delimited between $-z_0$ and z_0, where $z_0 = h/2$.

Indeed, the probe molecule is assumed to be hydrophobic, and therefore it is repelled by the polar faces of the membrane. To represent in a continuous form these enclosure and hydrophobicity effects, we assume that both ends of the molecule (which is also regarded as a "dumbbell") interact with the boundaries through a potential $V_{encl} = V_{encl}(z_1) + V_{encl}(z_2)$, where

$$V_{encl}(z_i) = kT \frac{K_z}{z_0^2 - z_i^2}, \qquad (2)$$

z_i being the z coordinate of bead i, with $i = 1, 2$. K_z is the constant for this potential. V_{encl} is rather flat in the interior of the membrane and grows rapidly to infinity when the molecule ends get close to the boundaries (see Fig. 1).

Equilibrium properties

The simplicity of the model allows a simple, statistical-mechanical treatment of the equilibrium properties. The instantaneous position of the molecule, the length of which is denoted as l, is specified by three coordinates: the position of the center of mass, z, and the polar angles of the molecule, θ and ϕ. These coordinates, along with the end-to-end distance, determine the position of the ends, from which the total potential energy can be calculated as
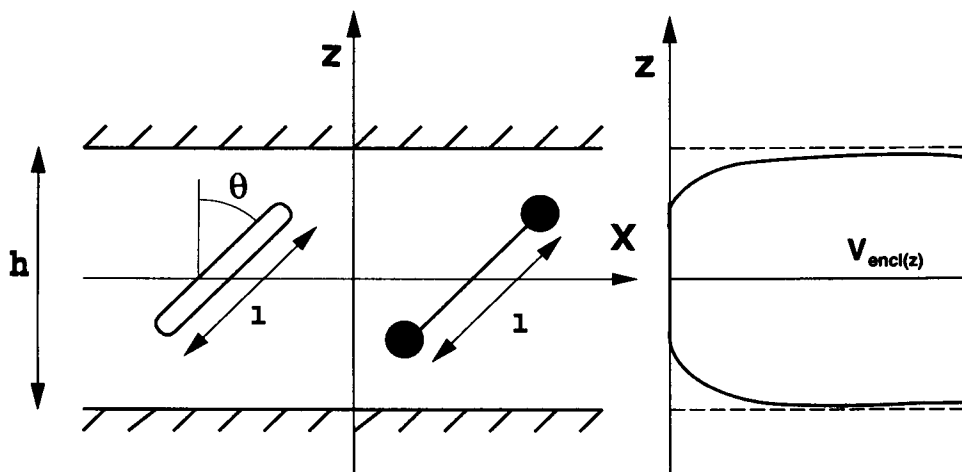
$$V(z, \theta) = V_{orient}(\theta) + V_{encl}(z_1) + V_{encl}(z_2), \qquad (3)$$

where $V(\theta)$ and $V(z_i)$ are given by Eqs. 1 and 2, respectively. The averages corresponding to observable quantities can be calculated through a statistical weight containing the Boltzmann factor $e^{-V/kT}$ and the geometric weight $\sin \theta$. An essential equilibrium property is the order parameter S, defined as

$$S \equiv \langle P_2(\cos \theta) \rangle, \qquad (4)$$

where $P_2(\cos \theta) \equiv (3\cos^2 \theta - 1)/2$ is the second Legendre polynomial. Thus S can be written in terms of the average $\langle \cos^2 \theta \rangle$. As we shall describe later, averages of other

FIGURE 1 Schematic representation of the membrane containing the probe molecule (shown in the two forms), illustrating the form of the enclosing potential.

Legendre polynomials are relevant to this problem, particularly $\langle P_1(\cos\theta)\rangle \equiv \langle\cos\theta\rangle$ and

$$\langle P_4(\cos\theta)\rangle \equiv \frac{1}{8}(35\langle\cos^4\theta\rangle - 30\langle\cos^2\theta\rangle + 3). \quad (5)$$

All of these averages can be expressed in terms of Equation

$$\langle\cos^n\theta\rangle = \frac{\int_{-z_0}^{z_0} dz \int_{\theta_{inf}}^{\theta_{sup}} d\theta \cos^n\theta \sin\theta e^{-V(z,\theta)/kT}}{\int_{-z_0}^{z_0} dz \int_{\theta_{inf}}^{\theta_{sup}} d\theta \sin\theta e^{-V(z,\theta)/kT}}. \quad (6)$$

(A trivial integration over ϕ, which cancels out, is omitted in Eq. 6.) The limits for the integration over θ in Eq. 6 are 0 and π (i.e., the full range of this angle), except when the molecule is quite close to the boundaries; actually, when $|z| > z_0 - (l/2)$, θ is limited to the interval between $\theta_{inf} = \theta_{lim}$ and $\theta_{sup} = \pi - \theta_{lim}$, where $\cos\theta_{lim} = (z_0 - |z|)/(l/2)$.

It may be interesting also to look at the distribution of the probe within the membrane, in regard to both orientation and position of the center of mass. This is given by the normalized probability density:

$$p(z,\theta) = \frac{\sin\theta e^{-V(z,\theta)/kT}}{\int_{-z_0}^{z_0} dz \int_{\theta_{inf}}^{\theta_{sup}} d\theta \sin\theta e^{-V(z,\theta)/kT}}. \quad (7)$$

We note that the geometrical weight, $\sin\theta$, is included in $p(z,\theta)$, along with the statistical weight (Boltzmann factor), $e^{-V(z,\theta)/kT}$.

The distribution of the center of mass can be obtained by integrating $p(z,\theta)$ over the angles:

$$f(z) = \frac{\int_{\theta_{inf}}^{\theta_{sup}} d\theta \sin\theta e^{-V(z,\theta)/kT}}{\int_{-z_0}^{z_0} dz \int_{\theta_{inf}}^{\theta_{sup}} d\theta \sin\theta e^{-V(z,\theta)/kT}}. \quad (8)$$

Furthermore, the orientational distribution function, which determines the probability that the θ angle takes some given value, regardless of the value of z, is formulated as

$$g(\theta) = \frac{\sin\theta \int_{-z_0}^{z_0} dz e^{-V(z,\theta)/kT} dz}{\int_{-z_0}^{z_0} \int_{\theta_{inf}}^{\theta_{sup}} d\theta \sin\theta e^{-V(z,\theta)/kT}}. \quad (9)$$

The double integrals involved in Eqs. 6–9 can be evaluated numerically. We used a subroutine based on Gauss quadratic fit, in which up to 60 quadrature points are placed in the integration interval. If the integral does not converge, the interval is halved, and the procedure is repeated for each subinterval.

There is a particular case that will be useful for the discussion of results; it corresponds to a hypothetical situation in which $V_{orient}(\theta) = 0$ and $V_{encl}(z_i) = 0$ for both beads. In this situation there is neither orienting potential nor enclosing potential, and the only restriction is that the probe must stay in the interior of the membrane, with the above-mentioned condition for the limits of θ. Then the Boltzmann factor is equal to unity and the integrals in Eqs. 6–9 can be calculated analytically. After some lengthy but straightforward calculus, we arrive at a general expression

for the averages of $\cos^n\theta$:

$$\langle\cos^n\theta\rangle = \begin{cases} \dfrac{h - l(n+1)/(n+2)}{(n+1)(h - l/2)} & \text{when } l \le h \\[4mm] \dfrac{2(h/l)^n}{(n+1)(n+2)} & \text{when } l \ge h \end{cases}. \quad (10)$$

From the result for $n = 2$ we evaluate the order parameter:

$$S = \begin{cases} \dfrac{-1}{8(h/l) - 4} & \text{when } l \le h \\[3mm] -1/4 & \text{when } l = h, \\[3mm] -\dfrac{1}{2}\left[1 - \dfrac{1}{2}(h/l)^2\right] & \text{when } l \ge h \end{cases} \quad (11)$$

and the distributions of z and θ can be also derived by integration. The results are

$$f(z) = \begin{cases} \dfrac{(h/2) - |z|}{(h/2)^2} & \text{when } l \ge h \\[4mm] \dfrac{1}{h - l/2} & \text{when } l \le h \text{ and } |z| \le z_0 - l/2 \\[4mm] \dfrac{h/2 - |z|}{(l/2)(h - l/2)} & \text{when } l \le h \text{ and } |z| \ge z_0 - l/2 \end{cases} \quad (12)$$

and

$g(\theta)$

$$= \begin{cases} \dfrac{\sin\theta(h - l\cos\theta)}{2h - l} & \text{when } l \le h \\[4mm] \dfrac{\sin\theta(h - l|\cos\theta|)}{h^2/l} & \text{when } l > h \text{ and } \theta_0 < \theta < \pi - \theta_0, \\[2mm] 0 & \text{when } l > h \text{ and } \theta < \theta_0 \text{ or } \theta > \pi - \theta_0 \end{cases} \quad (13)$$

where $\theta_0 = \arccos(h/l)$.

Dynamic properties

In the present study we characterize the reorientational dynamics of the probe molecule in terms of the correlation function,

$$\langle P_2(t)\rangle \equiv \langle P_2(\mathbf{u}(t)\cdot\mathbf{u}(0))\rangle, \quad (14)$$

where $\mathbf{u}(0)$ is the unitary vector along the probe axis at some (initial) time, and $\mathbf{u}(t)$ is the same after a time t has elapsed. The average in Eq. 14 refers to a collective of probe molecules. It can also be calculated from simulation as the average over all of the possible choices of the initial time along the Brownian trajectory of a single molecule. Note that $\mathbf{u}(t)\cdot\mathbf{u}(0) = \cos\psi(0,t)$, where ψ is the angle subtended by the orientations of the probe at times 0 and t.

The $\langle P_2(t)\rangle$ function is related to the decay of fluorescence anisotropy, $r(t)$, in experiments with fluorescent probes. Actually, when either the absorption or the emission dipole is along the molecule axis, $\langle P_2(t)\rangle$ is the normalized decay, i.e., $\langle P_2(t)\rangle = r(t)/r(0)$. Otherwise, a minor modifi-

cation is required. $\langle P_2(t) \rangle$ also determines the nuclear magnetic resonance relaxation (Lipari and Szabo, 1980). It is clear that $\langle P_2(0) \rangle = 1$, whereas when $t \to \infty$, $\langle P_2(t) \rangle \to \langle P_2 \rangle^2$, where $\langle P_2 \rangle \equiv S$ is the equilibrium order parameter (Eq. 4). Thus $\langle P_2(t) \rangle$ decays from 1 to S^2. Szabo (1984) and van der Meer et al. (1984) proposed a theoretical approximate treatment in which the correlation function is expressed in a model-independent way, in terms of only three parameters that have a well-defined meaning, regardless of the physical model. These are:

The rotational diffusion coefficient of the probe in an isotropic medium of the same effective viscosity, in the absence of any orienting effect, $D_r^\perp$.

The equilibrium values $\langle P_2 \rangle$ ($\equiv S$) and $\langle P_4 \rangle$ (Eqs. 4 and 5)

The theoretical expressions are (in our own notation)

$$\langle P_2(t) \rangle = a_0 + a_1 \exp(-b_1 t) + a_2 \exp(-b_2 t)$$
$$+ a_3 \exp(-b_3 t), \quad (15)$$

where

$$a_0 = \langle P_2 \rangle^2 = S^2 \quad (16)$$

$$a_1 = (1/5) + (2/7)\langle P_2 \rangle + (18/35)\langle P_4 \rangle - \langle P_2 \rangle^2 \quad (17)$$

$$a_2 = (1/5) + (1/7)\langle P_2 \rangle - (12/35)\langle P_4 \rangle \quad (18)$$

$$a_3 = (1/5) - (2/7)\langle P_2 \rangle + (3/35)\langle P_4 \rangle \quad (19)$$

and

$$b_1 = 6D_r^\perp[(1/5) + (1/7)\langle P_2 \rangle - (12/35)\langle P_4 \rangle]a_1^{-1} \quad (20)$$

$$b_2 = 6D_r^\perp[(1/5) + (1/14)\langle P_2 \rangle + (8/35)\langle P_4 \rangle]a_2^{-1} \quad (21)$$

$$b_3 = 6D_r^\perp[(1/5) - (1/7)\langle P_2 \rangle - (2/35)\langle P_4 \rangle]a_3^{-1} \quad (22)$$

We are also interested in the translational diffusivity of the probe. This is characterized by the mean squared displacement of the coordinates of the center of mass in some time t. For the α coordinate ($\alpha = x,y,z$), this is given by $\langle [\alpha(t) - \alpha(0)]^2 \rangle$, where the average is over the choice of the initial time. In free diffusion, for an unbound, randomly oriented particle, which does not experience any kind of potential, $\langle [\alpha(t) - \alpha(0)]^2 \rangle = 2D_t t$, where D_t is the (isotropic) translational diffusion coefficient.

In the present problem, we expect that lateral diffusion in the x and y direction is free, so that a similar relationship will hold:

$$\langle [x(t) - x(0)]^2 \rangle = 2D_{lat} t, \quad (23)$$

where D_{lat} is a lateral diffusion coefficient. The same will be valid for the y direction. However, motion in the transversal, z direction is bounded and restricted by the enclosing V_{encl} potential, so that $\langle [z(t) - z(0)]^2 \rangle$ will be a more complex function of time.

Still, the relationship between the free-diffusion translational friction coefficients and the observable, lateral or

transversal diffusion coefficients has to be determined. This, along with the description of the shape of the $\langle [z(t) - z(0)]^2 \rangle$ function, is one of the contributions of the present work and will be presented in the discussion of the results.

Brownian dynamics simulation

For simplicity, the probe is regarded dynamically as a dumbbell formed by two beads that are the frictional elements, joined by a frictionless connector of length l. For convenience in our simulation procedure, the connector is not absolutely rigid; instead, it behaves as a stiff spring with a Hookean potential, $V(b)/kT = H(b - l)^2$, where b is the instantaneous length, so that l is actually the equilibrium length. A high value, $H = 100kT/l$, is assigned to the stretching constant, for which the rms length, $\langle b^2 \rangle^{1/2} = 1.025l$, is only 2.5% larger than l.

The beads, the radius of which is σ, have a Stokes' law friction coefficient $\zeta = s\pi\eta\sigma$, where $s = 6$ or 4, respectively, for stick or slip boundary conditions. (Actually, our computer program was adapted from other codes designed for macromolecules, so that we took $\zeta = 6\pi\eta\sigma'$, where $\sigma' = \sigma$ or $\sigma' = 4\sigma/6$, depending on the boundary condition. In any case, the way in which we shall present the results makes the conclusions independent of the choice of the boundary condition.) The effective viscosity, η, is assumed to be uniform within the membrane. Hydrodynamic interaction between the two beads was included in the simulation using a modified Oseen tensor (Rotne and Prager, 1969; Yamakawa, 1970).

The simulation algorithm is that proposed by Ermak and McCammon (1978), with a predictor-corrector modification described by Iniesta and García de la Torre (1990). The computer program works with reduced, dimensionless quantities, that are also useful for the presentation of results. In particular, lengths are reduced with the probe length l. The unit of translational diffusion is kT/ζ. Thus, real time, t, is transformed into reduced time by

$$t^* = \left(\frac{kT}{\zeta l^2}\right) t. \quad (24)$$

Trajectories typically of $5-10 \times 10^6$ steps, with time step $\Delta t^* = 10^{-4}$, were simulated employing this procedure. The simulated trajectories are statistically analyzed to extract equilibrium properties, such as the averages in Eqs. 5 and 6 as well as the probability densities $p(\theta)$ and $f(z)$. From the trajectories we also extract the correlation functions, which are evaluated at selected times. The trajectory actually consists of $N_r + 1$ records (each containing the six bead coordinates), indexed as $j = 0, 1, \ldots N_r$, and the time interval between records is $\Delta t'$. Time is discretized as $t = j\Delta t'$, and the average in Eq. 14 is evaluated in the discrete form:

$$\langle P_2(j\Delta t') \rangle = \frac{1}{N_r - j + 1} \sum_{i=0}^{N_r - j} \langle P_2(\mathbf{u}_{i+j} \cdot \mathbf{u}_i) \rangle. \quad (25)$$

The numerical values of the $\langle P_2(t) \rangle$ function are submitted to a multiexponential fit based on the DISCRETE procedure developed by Provencher (1976a,b). Thus the fitting function includes a baseline:

$$\langle P_2(t) \rangle = a_0 + a_a \exp(-b_a t) + a_b \exp(-b_b t) + \cdots \quad (26)$$

The amplitudes and time constants are now denoted a_a, a_b, a_c... and b_a, b_b, b_c... to distinguish them from the series a_1, a_2, a_3... and b_1, b_2, b_3... that appear in the theoretical expressions like Eqs. 15–22.

Free-particle diffusion coefficients

The instantaneous diffusivity of any particle is given by the translational and rotational diffusion tensors, $\mathbf{D}_t$ and $\mathbf{D}_r$, the components of which obviously depend on the system of reference axes. For an axisymmetric particle, in a particle-fixed system of coordinates, we have $\mathbf{D}_t = \text{diag}(D_t^{\perp}, D_t^{\perp}, D_t^{\|})$, and $\mathbf{D}_r = \text{diag}(D_r^{\perp}, D_r^{\perp}, D_r^{\|})$, where diag(...) means a diagonal 3×3 matrix with the mentioned components. For isotropic translation of a free particle, the overall diffusion coefficient is $D_t = (2D_t^{\perp} + D_t^{\|})/3$, whereas the end-over-end rotation of an axially symmetric particle is determined by $D_r^{\perp}$.

From elementary hydrodynamics (Happel and Brenner, 1973; García de la Torre and Bloomfield, 1980) the translational and rotational diffusion coefficients can be calculated. As the hydrodynamic interaction effect is taken into account, both coefficients depend on the ratio $\zeta/6\pi\eta l$ and have to be calculated numerically. For our dumbbell, the case with strongest hydrodynamic interaction that we consider corresponds to $\sigma_1 = \sigma_2 = l/2$, i.e., when the beads are tangent. Numerical calculation (García de la Torre and Bloomfield, 1980) gives, for this case, $D_t^{\perp *} = 0.71875$, $D_t^{\| *} = 0.8125$, which leads to $D_t^* = 0.75$, and $D_r^{\perp *} = 1.125$, where the latest value does not include the so-called volume correction for rotational diffusion (García de la Torre and Rodes, 1983), for consistency with the BD methodology.

RESULTS AND DISCUSSION

Equilibrium properties

As an example of the analytical results that we found for the confined probe, without other potentials, we present in Fig. 2 the variation of the order parameter with the membrane-to-probe length ratio, h/l. We first note that S is always negative. In practice, the effect from enclosure will not act alone, but combines instead with the orienting effect due to the phospholipid tails. Then the contribution from confinement will be to lower S, to a larger extent for longer probe molecules. However, in a number of cases of interest, h/l may be typically 2–4, for which the contribution to S due to confinement will be only about -0.1, as seen in Fig. 2.

An example of the probability density, $p(z,\theta)$, is displayed in Fig. 3. There are twin peaks corresponding to the
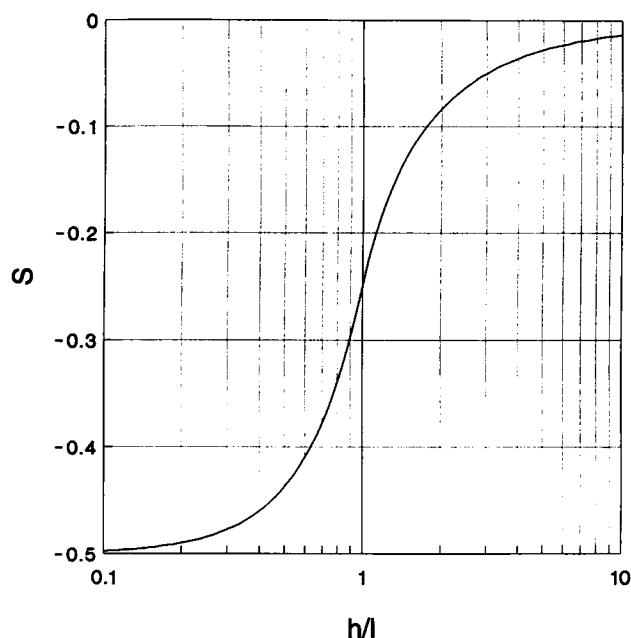

FIGURE 2   Order parameter S for a confined probe, without other potentials, plotted versus the membrane height to probe length ratio, h/l.

most probable values of θ and its supplementary, and to the middle of the membrane. We note that for $\theta = \pi/2$, when all the z positions are possible, the distribution is rather flat; the probability falls to zero just near the borders of the membrane. This situation is only slightly sensitive to the value of K_z when this constant takes moderate values $K_z = 0 - 2$.

Examples of the orientational distributions, $g(\theta)$, are presented in Fig. 4. We note that the effect of increasing the enclosing constant, K_z, is to increase the probability that $\theta \approx \pi/2$. In this situation the probe molecule is preferentially horizontal, i.e., parallel to the faces of the membrane, as a result of the hydrophobic repulsion by the walls. On the other hand, for null or moderate values of K_z, the effect of increasing K_θ is the appearance of maxima of probability for $\theta \approx 0$ and $\theta \approx \pi$, for which the probe is nearly vertical.
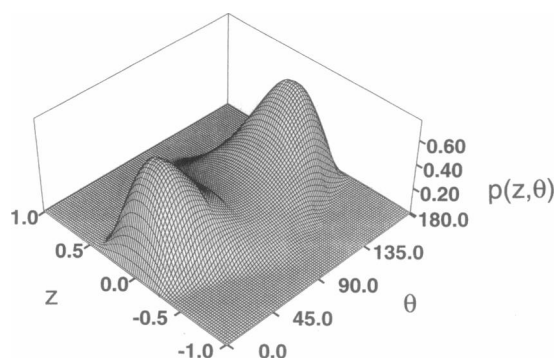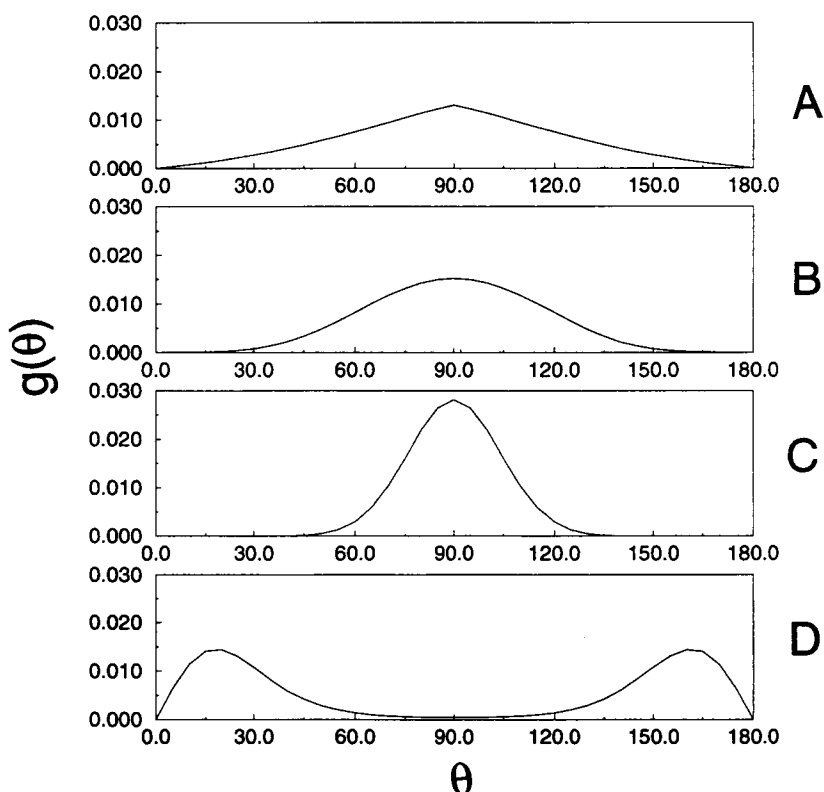

FIGURE 3   Three-dimensional plot of the probability density, $p(\theta,z)$, versus θ and z, for a case with $h/l = 2$, $K_\theta = 2$, and $K_z = 1$.

FIGURE 4 Angular distribution, $g(\theta)$ versus θ, for the following cases. (A) $K_\theta = 0$ and $K_z = 0$. (B) $K_\theta = 2$ and $K_z = 2$. (C) $K_\theta = 4$ and $K_z = 0$. (D) $K_\theta = 0$ and $K_z = 4$. In all cases, $h/l = 1.5$.

We may also consider the variation of the experimentally observable order parameter, S, with the three parameters, h/l, K_z, and K_θ. Some examples are presented in Fig. 5. We see that for a probe that is not too long, the variation with K_z is insignificant. Thus it may be reasonable to wait for others to fix this constant to a moderate value, say $K_z = 1 - 2$, and focus our attention on the variation with probe length and orienting constant.

In Table 1 we list values of the order parameter calculated for various values of the model constants. We see, as expected, that the effect of increasing l (decreasing h/l) is a decrease in S, whereas an increase in K_θ obviously increases S. This leads to an important conclusion: the combination of the usual Maier-Saupe potential with an enclosing potential may produce a cancellation of effects, so that the order parameter $\langle P_2(\cos \theta) \rangle$ can equal zero for certain values of the model parameters. This has important implications for the interpretation of experimental results: a probe might look "disordered," as if it had a flat, uniform orientational distribution, when actually it interacts strongly with its environment, having perhaps a bimodal angular distribution. The distinction between these two cases requires the measurement of $\langle P_4(\cos \theta) \rangle$, which would be nonzero in the latter case.

The above examples suffice to illustrate the effects of enclosure, hydrophobicity, and orienting environment on the spatial position of the probe within the membrane. Any other cases can be straightforwardly computed using our analytical results or by numerical integration.

Dynamic properties: trajectories and averages

It is instructive to look at time evolution, along the simulated BD trajectory, of the position of the center of the probe, z, and its orientation given by $\cos \theta$. These time series give a pictorial description of the Brownian motion of the probe within the membrane. Figs. 6 and 7 illustrate some examples.

Fig. 6 shows the trace of $\cos \theta$ for various simulations with different angular constants, K_θ. As this constant is increased, the potential barrier at $\cos \theta = \pi/2$ is higher, and the system tends to reside near either $\theta \approx 0$ or $\theta \approx \pi$. The number of transitions between these two states, observed in a given time (30 reduced units in Fig. 6), is smaller for larger K_θ.

The evolution of the center of mass is similarly displayed in Fig. 7. In the absence of potentials, z fluctuates widely and frequently between the two extremes (walls). However, when K_z or the l/h ratio is increased, the center of the probe is preferentially near the center of the membrane and fluctuates more slowly.

From the statistical analysis of the trajectories we obtain averages that can be compared with those obtained by direct integration. The later procedure is obviously more immediate and much less time consuming. The only purpose of this is to check the BD simulation procedure and working conditions. Table 1 presents such a comparison in a few cases. The BD averages were obtained from a trajectory of 1,500,000 steps divided into five subtrajectories. We note
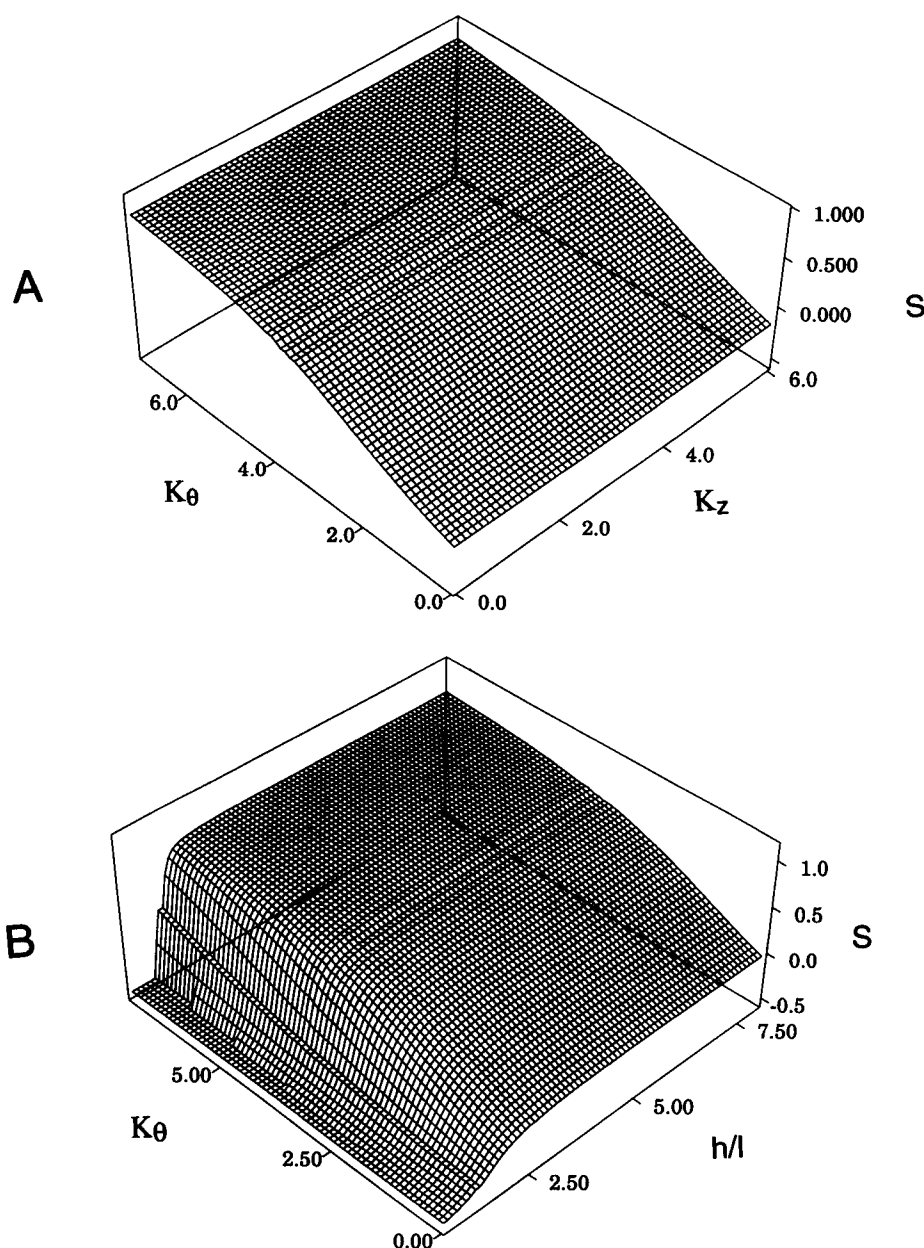
FIGURE 5 Three-dimensional plots of the order parameter S as a function of two of the constants for a fixed value of the third one. (A) Variation with K_z and K_θ for fixed $h/l = 2$. (B) Variation with h/l and K_θ for fixed $K_z = 1$.

that the BD results coincide well with the numerical results, within their statistical error. This is a good check of the performance of both procedures.

Dynamic properties: rotational diffusion

The $\langle P_2(t) \rangle$ function, defined by Eq. 14, was computed from the Brownian trajectories according to Eq. 25. Typically we carried out trajectories of $1 - 5 * 10^6$ steps, with a total duration of 100–500 units of reduced time. Examples of the results are presented in Fig. 8. The curves show the expected asymptotic behavior at long times, with $\langle P_2(\infty) \rangle = S^2$, and the S values obtained from the asymptote are in good agreement with those from other procedures (Table 1).

The simulated $\langle P_2(t) \rangle$ results were compared with the theoretical equations from the model-free approach (Lipari and Szabo, 1980; Szabo, 1984; van der Meer, 1984). The agreement is rather good, except for a minor deviation noticed at intermediate times in some cases (like B in Fig. 8). We have included in Fig. 8 a rather interesting example of the situation described above, in which the orienting effects of K_θ and K_z are moderately strong but, because of their opposite direction, they cancel each other in such a way that $\langle S \rangle \simeq 0$, as for a free molecule. Then we see in this case (curve D in Fig. 8) that the whole decay is nearly the same as for a free molecule, although the angle distribution, $g(\theta)$, is quite different.

The kinetics of the $\langle P_2(t) \rangle$ decays can be characterized in terms of two characteristic relaxation times. One of them is

TABLE 1   Comparison of values of $\langle P_2(\cos\theta)\rangle$ **and** $\langle P_4(\cos\theta)\rangle$ **obtained from theoretical expressions and from Brownian dynamics simulation**

l/h	K_θ	K_z	$\langle P_2(\cos\theta)\rangle$		$\langle P_4(\cos\theta)\rangle$	
			Simulation	Theory	Simulation	Theory
0.25	3.0	1.0	0.581 ± 0.019	0.582	0.232 ± 0.016	0.228
0.25	5.0	1.0	0.760 ± 0.003	0.769	0.436 ± 0.008	0.441
0.25	0.0	3.0	-0.066 ± 0.049	-0.041	0.003 ± 0.014	0.002
0.25	5.0	3.0	0.773 ± 0.008	0.766	0.447 ± 0.011	0.437
0.25	5.0	5.0	0.755 ± 0.008	0.764	0.422 ± 0.011	0.433
0.5	0.0	1.0	-0.171 ± 0.023	-0.153	0.021 ± 0.017	0.018
0.5	3.0	1.0	0.451 ± 0.012	0.458	0.117 ± 0.014	0.134
0.5	5.0	1.0	0.723 ± 0.005	0.718	0.371 ± 0.013	0.367
0.5	0.0	3.0	-0.260 ± 0.009	-0.247	0.058 ± 0.007	0.048
0.5	5.0	3.0	0.644 ± 0.021	0.624	0.267 ± 0.020	0.254
0.5	5.0	5.0	0.504 ± 0.027	0.490	0.164 ± 0.022	0.134
0.91	0.0	1.0	-0.423 ± 0.001	-0.422	0.215 ± 0.003	0.211
0.91	3.0	1.0	-0.370 ± 0.005	-0.376	0.136 ± 0.007	0.137
0.91	5.0	1.0	-0.283 ± 0.010	-0.321	0.048 ± 0.009	0.058
0.91	0.0	3.0	-0.463 ± 0.000	-0.464	0.291 ± 0.001	0.292
0.91	5.0	3.0	-0.455 ± 0.001	-0.448	0.254 ± 0.003	0.258

the initial relaxation time, τ_{ini}, which describes the initial rate of decay:

$$\tau_{ini} = -[(d \ln\langle P_2(t)\rangle/dt)_{t=0}]^{-1}, \qquad (27)$$

and the other one is the mean relaxation time, τ_{mean}, given by Equation 28

$$\tau_{mean} = (1 - a_0)^{-1}\int_0^\infty [\langle P_2(t)\rangle - \langle P_2(\infty)\rangle]dt, \qquad (28)$$

which indicates an average rate of a normalized decay (from 1 to 0) through the full curve. Note that τ_{mean} equals the inverse of the area between the curve and the asymptote.

On the theoretical side, the application of the definition of τ_{ini} to the three-exponential approximation, Eq. 15, leads to Equation 29

$$\tau_{ini} = (a_1b_1 + a_2b_2 + a_3b_3)^{-1} = (6D_r^\perp)^{-1} \qquad (29)$$

$$\tau_{mean} = (a_1/b_1 + a_2/b_2 + a_3/b_3)/(1 - a_0). \qquad (30)$$

The result that $\tau_{ini} = (6D_r^\perp)^{-1}$ is obtained from Eqs. 16–22 after some algebraic manipulations. In reduced units (see Eq. 24), we have $\tau_{ini}{}^* = 1/12 = 0.0833$ for the no-HI case, and $\tau_{ini}{}^* = 0.148$ in the HI case specified above. The simulated $\langle P_2(t)\rangle$ curve at short times was fitted to a quadratic or cubic equation in t, and τ_{ini} was calculated from the linear coefficient. In a number of cases that we examined, the simulated τ_{ini} was in very good agreement with the theoretical results, with deviations typically smaller than 5%. We also notice from Fig. 8 that the initial slope is the same in all cases.

From the multiexponential fit of the simulated $\langle P_2(t)\rangle$ decays, we have obtained the mean relaxation times, given now by $\tau_{mean} = (a_a/b_a + a_b/b_b + \ldots)/(1 - a_0)$. In Fig. 9 we

present a comparison of theory and simulation in some cases. The agreement is quite good, and we notice that the theory describes well the deviation of τ_{mean} from the free-molecule value. The model-free approach for rotational diffusion had been found to work rather well for problems in which the orientation was represented by simple potentials, $V(\theta)$, depending on the orientation of the probe (see, for instance, López Martínez and García de la Torre, 1987). In the present work we find that the good performance remains for a more complex orienting situation in which the potential, $V(z,\theta)$, depends not only on orientation but also on position.

Dynamic properties: translational diffusion

The instantaneous diffusivity of any particle is given by the translational and rotational diffusion tensors, $\mathbf{D}_t$ and $\mathbf{D}_r$, the components of which obviously depend on the system of reference axes. For an axisymmetric particle, in a particle-fixed system of coordinates, we have $\mathbf{D}_t = \text{diag}(D_t^\perp, D_t^\perp, D_t^\|)$, and $\mathbf{D}_r = \text{diag}(D_r^\perp, D_r^\perp, D_r^\|)$, where $\text{diag}(\ldots)$ means a diagonal 3×3 matrix with the mentioned components.

For isotropic translation, the overall diffusion coefficient is $D_t = (2D_t^\perp + D_t^\|)/3$. However, this coefficient will not hold for diffusion in the membrane interior, but instead a lateral diffusion coefficient D_{lat} should be used, as described above. In an instantaneous orientation of the particle, the lateral diffusivity in the x or y directions is given by the D_t^{xx} or D_t^{yy} components, respectively, of $\mathbf{D}_t$ in the lab-fixed system of coordinates. Similarly, the instantaneous diffusivity in the direction perpendicular to the membrane plane will be D_t^{zz}. The $\mathbf{D}_t$ tensor can be transformed from the particle-fixed system to the lab-fixed system, which yields
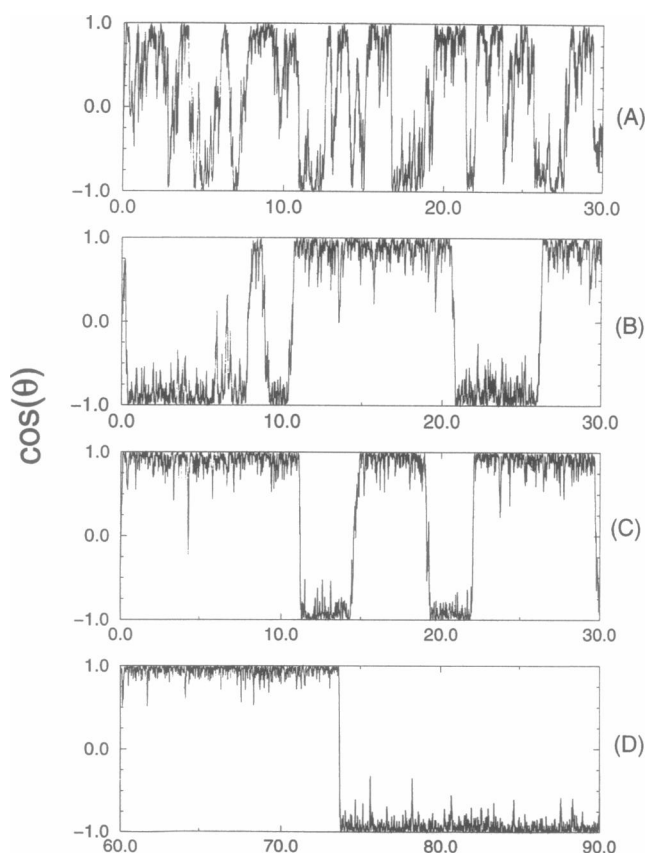
FIGURE 6   Evolution of cos θ along a portion of a Brownian trajectory of 30 units of reduced time. Cases: (A) $h/l = 2$, $K_z = 1$, $K_\theta = 2$. (B) $h/l = 2$, $K_z = 1$, $K_\theta = 3.5$. (C) $h/l = 2$, $K_z = 1$, $K_\theta = 5$. (D) $h/l = 2$, $K_z = 1$, $K_\theta = 7$.
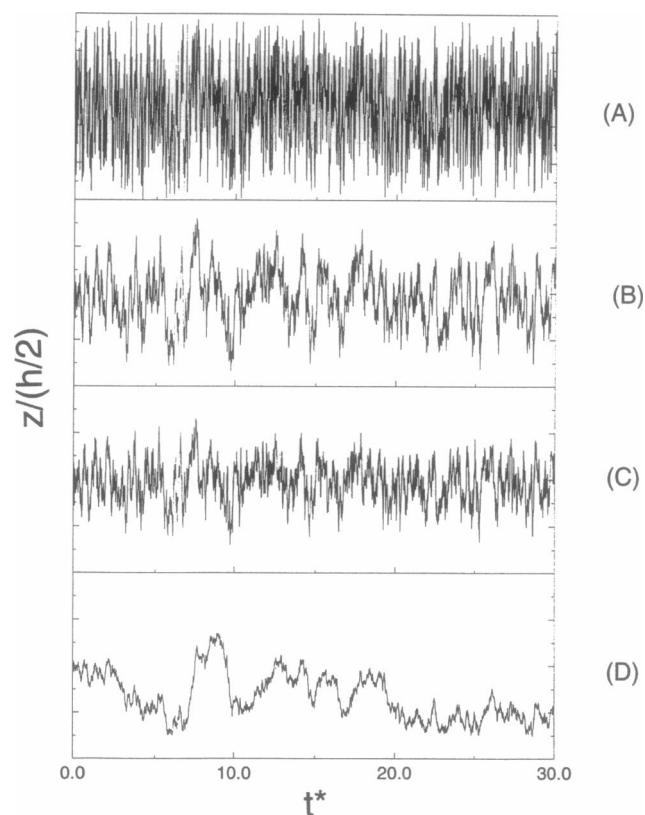

FIGURE 7   Evolution of z along a portion of a Brownian trajectory of 30 units of reduced time. Cases: (A) $h/l = 0.5$, $K_z = 0$, $K_\theta = 0$. (B) $h/l = 2$, $K_z = 1$, $K_\theta = 0$. (C) $h/l = 2$, $K_z = 3$, $K_\theta = 0$. (D) $h/l = 6$, $K_z = 0$, $K_\theta = 0$.

expressions for D_t^{xx} and D_t^{zz} containing $D_t^\perp$ and $D_t^\parallel$, along with the terms $\cos^2\theta$ and $\cos^2\phi$, where ϕ is the azimuthal angle that describes, along with θ, the orientation of the probe.

The average translational diffusivity can be obtained by averaging over orientations. It is clear that $\langle\cos^2\theta\rangle$ depends, as described above, on the membrane parameters, whereas $\langle\cos^2\phi\rangle = 0$ because of the symmetry around axis z. Thus the results are finally simplified to

$$D_{lat} \equiv \langle D_t^{xx}\rangle = \frac{1}{2}\left[D_t^\perp(1 + \langle\cos^2\theta\rangle) + D_t^\parallel(1 - \langle\cos^2\theta\rangle)\right] \tag{31}$$

$$D_{transv} \equiv \langle D_t^{zz}\rangle = D_t^\perp(1 - \langle\cos^2\theta\rangle) + D_t^\parallel\langle\cos^2\theta\rangle. \tag{32}$$

From the Brownian trajectory of the probe molecule, correlation functions can be calculated for the square displacement of the center of mass. The x and y coordinates are unbound, and therefore we predict an Einsteinian behavior, with a diffusion coefficient D_{lat}:

$$\langle[x(t) - x(0)]^2\rangle = 2D_{lat}t, \tag{33}$$

valid for any time. The same relationship holds for the y coordinate. However, the motion is limited in the z direc-

tion. For short times, the trajectory of the molecule will not be (on the average) long enough to reach the walls of the membrane, and therefore a similar expression is expected for z, now with the transversal coefficient, D_{transv}:

$$\langle[z(t) - z(0)]^2\rangle = 2D_{transv}t \quad (t \to 0). \tag{34}$$

On the other hand, if t is very long, the final position is not correlated with the initial one; $z(t) - z(0)$ is the z distance from two arbitrary points within the membrane, δ_z (each obeying the probability density $f(z)$); and the correlation function tends to a constant,

$$\langle[z(t) - z(0)]^2\rangle = \langle\delta_z^2\rangle \quad (t \to \infty). \tag{35}$$

$\langle\delta_z^2\rangle$ is an equilibrium average that could be calculated if the distributions $f(z)$ were known.

From our simulations, the validity of our predictions for translational diffusion, Eqs. 33 and 35, can be ascertained. Fig. 10 shows an example of the time dependence of the correlation functions, which is found to be as predicted, i.e., a straight line for x and a plateau-reaching curve for z. From a least-squares analysis of the very first data points, we can obtain the initial slopes, $2D_{lat}$ and $2D_{transv}$. Fig. 11 displays an example of these short-time values. The results so ob-
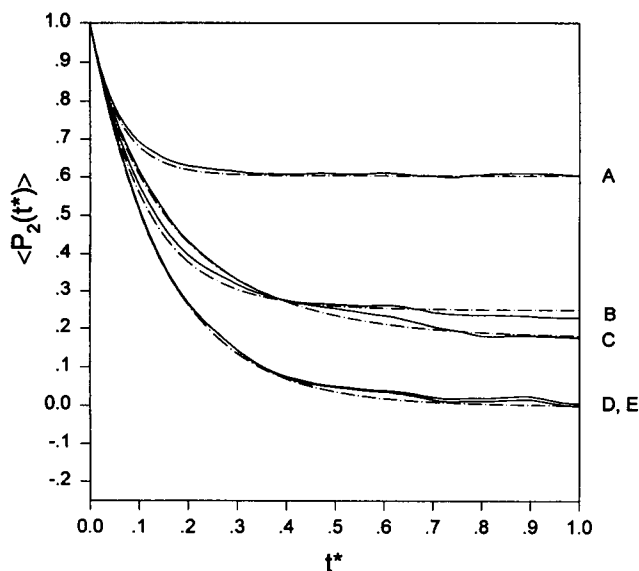
FIGURE 8 Decay of the correlation function $\langle P_2(t) \rangle$ with reduced time t^*. Continuous curves: simulation results with HI; dotted curves: theoretical approximation. Cases: (A) $h/l = 999$, $K_z = 0$, $K_\theta = 5$. (B) $h/l = 2$, $K_z = 1$, $K_\theta = 3.23$. (C) $h/l = 1$, $K_z = 1$, $K_\theta = 3$. (D) $h/l = 2$, $K_z = 3$, $K_\theta = 1.74$. (E) $h/l = 999$, $K_z = 0$, $K_\theta = 0$. The lowest dashed curve is the decay for a free molecule, $\langle P_2(t) \rangle = \exp(-6D_r^\perp{}^* t^*)$.

FIGURE 10 Translational correlation functions $\langle [x(t) - x(0)]^2 \rangle$ and $\langle [z(t) - z(0)]^2 \rangle$ versus reduced time t^*, for $h/l = 2$, $K_z = 1$, $K_\theta = 3.23$.

CONCLUSIONS

tained from simulations for D_{lat} and D_{transv} were compared with our theoretical results, Eqs. 31 and 32, in which the $\langle \cos^2\theta \rangle$ values were calculated by numerical integration. The inclusion of hydrodynamic interaction in our simulation was essential, because otherwise D_t is isotropic and D_{lat} and D_{transv} would coincide. The comparison shows an excellent agreement between simulation and theory, with differences that are on the order of 1% only, in most of the cases examined.
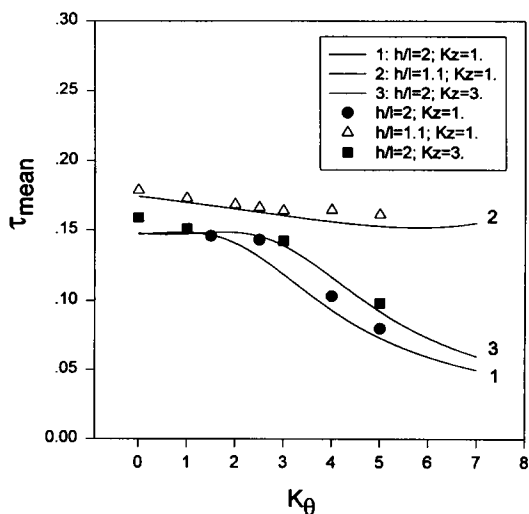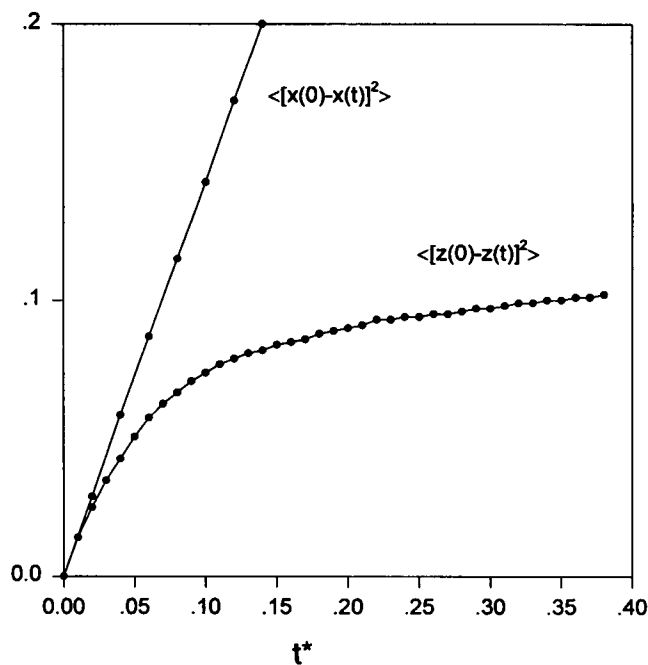
We have proposed a simple model for the behavior of a probe molecule embedded in a membrane. In addition to a Maier-Saupe potential, the probe-membrane interaction includes an enclosing potential. Thanks to the simplified
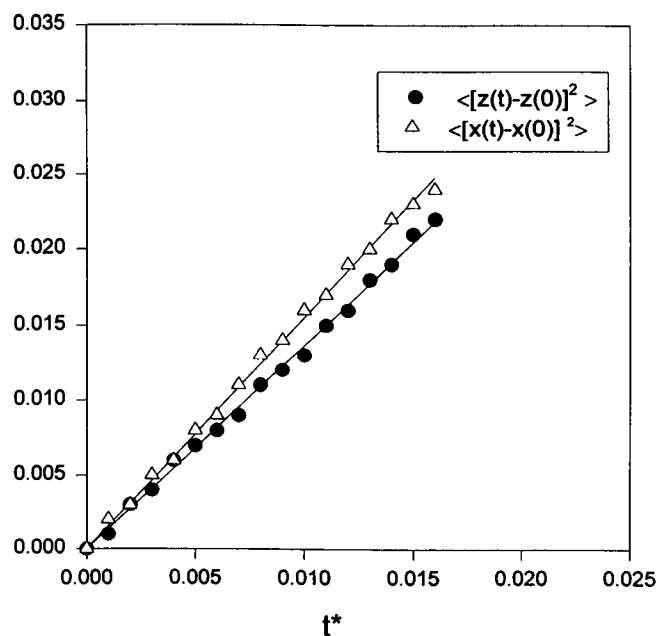

FIGURE 9 Mean relaxation times, τ_{mean}, versus K_θ for some cases with the indicated K_z and h/l. The continuous lines are the predictions of the theoretical approximation and the date points are simulation results.

FIGURE 11 Short-time behavior or the translational correlation functions $\langle [x(t) - x(0)]^2 \rangle$ and $\langle [z(t) - z(0)[^2 \rangle$ versus reduced time t^*, for $h/l = 0.7$, $K_z = 0$, $K_\theta = 0$. The same as in Fig. 9, for very short times, showing the initial slopes.

description of the geometry and the energetics of the system, a statistical-mechanical treatment can be easily constructed that gives an intuitive description of the equilibrium behavior and allows an easy calculation of properties like the distribution functions $p(z,\theta)$, $g(\theta)$, and $f(z)$, as well as the order parameter. An important finding is that, because of cancellation of the opposite effects of the two contributions to the potential, zero-order parameters may result, even for strongly ordered systems.

The simulation of the Brownian dynamics of the model is also quite feasible and provides us with results for the correlation functions for rotation, $\langle P_2(t) \rangle$, and translation, $\langle [x(t) - x(0)]^2 \rangle$ and $\langle [z(t) - z(0)]^2 \rangle$. A model-free theoretical approach available in the literature for rotational diffusion has been found to be in good agreement with simulations. For translational diffusion, we define diffusion coefficients D_{lat} and D_{transv} and express their values in terms of the free-particle translational diffusion tensor and the orientational statistics of the probe. These values determine the initial slope of the translational correlation functions, as found by comparison of calculated and simulated values. In summary, for translation as well as for rotation, it is possible to predict the dynamic behavior of the probe in the membrane from the free-particle diffusion coefficients and equilibrium averages like $\langle \cos^2\theta \rangle$ and $\langle \cos^4\theta \rangle$, which can be obtained from separate, nondynamic calculations or experiments.

REFERENCES

Ameloot, M., H. Hendricks, W. Herreman, H. Pottel, and W. Van der Meer. 1984. Effect of orientational order on the decay of the fluorescence anisotropy in membrane suspensions. Experimental verification. *Biophys. J.* 46:525–539.

Basolino-Klimas, D., H. E. Alper, and T. R. Stouch. 1993. Solute diffusion in lipid bilayer membranes: an atomic level study by molecular dynamics. *Biochemistry.* 32:12624–12637.

Bayley, P. M., and R. Dale, editors. 1985. Spectroscopy and the Dynamics of Molecular Biological Systems. Academic, New York.

de Loof, H., S. C. Harvey, J. P. Segrest, and R. W. Pastor. 1990. Mean field stochastic boundary molecular dynamics simulation of a phospholipid in a membrane. *Biochemistry.* 8:2209–2113.

Egberts, E., and H. J. C. Berendsen. 1994. Molecular dynamics simulation of a phospholipid membrane. *Eur. Biophys. J.* 22:423–436.

Eisinger, J., and S. F. Scarlata. 1987. The lateral fluidity of erythrocyte membranes. Temperature and pressure dependence. *Biophys. Chem.* 28:273–281.

Ermak, D. L., and J. A. McCammon. 1978. Brownian dynamics with hydrodynamic interactions. *J. Chem. Phys.* 69:1352–1357.

Galla, H. J., and E. Sackman. 1974. Lateral diffusion in the hydrophobic region of membranes. Use of pyrene excimers as optical probes. *Biochem. Biophys. Acta.* 339:103–115.

García de la Torre, J., and V. A. Bloomfield. 1980. Hydrodynamic properties of complex, rigid, biological macromolecules. *Q. Rev. Biophys.* 14:81–139.

García de la Torre, J., and V. Rodes. 1983. Effects from bead size and hydrodynamic interaction on the translational and rotational coefficients of macromolecular bead models. *J. Chem. Phys.* 79:2454–2460.

Happel, A., and H. Brenner. 1973. Low Reynolds Number Hydrodynamics. Nordhoff, Leiden.

Iniesta, A., and J. García de la Torre. 1990. A second-order algorithm for the simulation of the Brownian dynamics of macromolecular models. *J. Chem. Phys.* 92:2015–2019.

Jovin, T. M., M. Bartholdi, W. L. C. Vaz, and R. H. Austin. 1981. Rotational diffusion of biological macromolecules by time-resolved delayed luminescence (phosphorescence, fluorescence) anisotropy. *Ann. N.Y. Acad. Sci.* 366:176–179.

Kinosita, K., S. Kawato, and A. Ikegami. 1977. A theory of fluorescence depolarization decay in membranes. *Biophys. J.* 20:289–299.

Lipari, G., and A. Szabo. 1980. Effect of librational motion on fluorescence depolarization and nuclear magnetic resonance relaxation in macromolecules and membranes. *Biophys. J.* 30:489–506.

Lipari, G., and A. Szabo. 1982. Model-free approach to the interpretation of nuclear magnetic resonance relaxation in macromolecules. I. Theory and range of validity. *J. Am. Chem. Soc.* 104:4564–4559.

Loew, L. M., editor. 1988. Spectroscopic Membrane Probes. CRC Press, Boca Raton.

Lopez Cascales, J. J., J. García de la Torre, S. J. Marrink, and H. J. C. Berendsen. 1996a. Molecular dynamics simulation of a charged biological membrane. *J. Chem. Phys.* 104:2713–2720.

Lopez Cascales, J. J., H. J. C. Berendsen, and J. García de la Torre. 1996b. Molecular dynamics simulation of water between two charged layers of dipalmitoylphosphatidylserine. *J. Phys. Chem.* 100:8621–8627.

López Martínez, M. C., and J. García de la Torre. 1987. Brownian dynamics simulation of restricted rotational diffusion. *Biophys. J.* 52:303–310.

Mateo, C. R., M. P. Lillo, J. Gonzalez-Rodriguez, and A. U. Acuña. 1991a. Molecular order and fluidity of the plasma membrane of human platelets from time-resolved fluorescence depolarization. *Eur. Biophys. J.* 20:41–52.

Mateo, C. R., M. P. Lillo, J. Gonzalez-Rodriguez, and A. U. Acuña. 1991b. Lateral heterogeneity in human platelet plasma membrane and lipids from the time-resolved fluorescence depolarization of trans-parinaric acid. *Eur. Biophys. J.* 20:53–61.

Mateo, C. R., P. Lillo, J. C. Brochon, M. Martinez-Ripoll, J. Sanz-Aparicio, and A. U. Acuña. 1993. Rotational dynamics of 1,6-diphenyl-1,3,5-hexatriene and derivatives from fluorescence despolarization. *J. Phys. Chem.* 97:3486–3491.

Pastor, R. P., and A. Szabo. 1992. Langevin dynamics of a linear rotor in the Maier-Saupe potential: Kramers turnover of the flipping rate. *J. Chem. Phys.* 97:5098–5100.

Pastor, R. P., and A. Szabo. 1994. Rotational relaxation in orienting potentials: theory and simulations. *In* Computer Simulation of Liquid Crystals. G. R. Luckhurst, editor. Kluwer Academic Publishers, Dordrecht, The Netherlands.

Pastor, R. W., and R. M. Venable. 1988. Brownian dynamics simulation of a lipid chain in a membrane bilayer. *J. Chem. Phys.* 89:1112–1127.

Pastor, R. W., and R. M. Venable. 1994. Molecular and stochastic dynamics simulation of lipid membranes. *In* Computer Simulations of Biomolecular Systems: Theoretical and Experimental Applications. W. van Gunsteren, P. K. Weiner, and A. K. Wilkinson, editors. ESCOM Science Publishers, Leiden, The Netherlands.

Pastor, R. W., R. M. Venable, M. Karplus, and A. Szabo. 1988. A simulation based model of NMR T1 relaxation in lipid bilayer vesicles. *J. Chem. Phys.* 89:1128–1140.

Provencher, S. 1976a. An eigenfunction expansion method for the analysis of exponential decay curves. *J. Chem. Phys.* 64:2772–2777.

Provencher, S. 1976b. A Fourier method for the analysis of exponential decay curves. *Biophys. J.* 16:151–170.

Rotne, J., and S. Prager. 1969. Variational treatment of hydrodynamic interaction in polymers. *J. Chem. Phys.* 50:4381–4386.

Saffman, P. G., and M. Delbrück. 1975. Brownian motion in biological membranes. *Proc. Natl. Acad. Sci. USA.* 72:3111–3113.

Szabo, A. 1984. Theory of fluorescence depolarization in macromolecules and membranes. *J. Chem. Phys.* 81:150–167.

van der Meer, W., H. Pottel, W. Herreman, M. Ameloot, H. Hendricks, and H. Schroder. 1984. Effect of orientational order on the decay of the fluorescence anisotropy in membrane suspensions. A new approximate solution of the rotational diffusion equation. *Biophys. J.* 46:525–539.

van der Ploeg, P., and H. J. C. Berendsen. 1982. Molecular dynamics simulation of a bilayer membrane. *J. Chem. Phys.* 76:3271–3277.

Venable, R. M., Y. Zhang, B. J. Hardy, and R. W. Pastor. 1993. Molecular dynamics simulation of a lipid bilayer and of hexadecane: an investigation of membrane fluidity. *Science.* 262:223–226.

Yamakawa, H. 1970. Transport properties of polymer chains in dilute solution: hydrodynamic interaction. *J. Chem. Phys.* 53:436–443.